ACS APPLIED MATERIALS & INTERFACES

Research Article

www.acsami.org

Pronounced Cosolvent Effects in Polymer:Polymer Bulk Heterojunction Solar Cells with Sulfur-Rich Electron-Donating and Imide-Containing Electron-Accepting Polymers

Sungho Nam,[†,‡] Sungho Woo,[§] Jooyeok Seo,[†] Wook Hyun Kim,[§] Hwajeong Kim,*[,†,∥] Christopher R. McNeill,[⊥] Tae Joo Shin,[#] Donal D. C. Bradley,[‡] and Youngkyoo Kim*[,†]

[†]Organic Nanoelectronics Laboratory, School of Applied Chemical Engineering, Kyungpook National University, Daegu 702-701, Republic of Korea

[‡]Center for Plastic Electronics, Department of Physics, Blackett Laboratory, Imperial College London, London SW7 2AZ, United Kingdom

[§]Green Energy Research Division, Daegu Gyeongbuk Institute of Science and Technology, Daegu 711-873, Republic of Korea

[∥]Research Institute of Advanced Energy Technology, Kyungpook National University, Daegu 702-701, Republic of Korea

[⊥]Department of Materials Engineering, Monash University, Victoria 3800, Australia

[#]SAXS Beamline, Pohang Accelerator Laboratory, Pohang 790-784, Republic of Korea

Supporting Information

ABSTRACT: The performance of solar cells with a polymer:polymer bulk heterojunction (BHJ) structure, consisting of poly[4,8-bis(5-(2-ethylhexyl)thiophen-2-yl)benzo[1,2-b:4,5-*b*′]dithiophene-*alt*-3-fluorothieno[3,4-*b*]thiophene-2-carboxylate] (PTB7-Th) donor and poly[[*N*,*N*′-bis(2-octyldodecyl)-naphthalene-1,4,5,8-bis(dicarboximide)-2,6-diyl]-*alt*-5,5′-(2,2′-bithiophene)] (P(NDI2OD-T2)) acceptor polymers, was investigated as a function of cosolvent (*p*-xylene:chlorobenzene (pXL:CB)) composition ratio. A remarkable efficiency improvement (~38%) was achieved by spin-coating the photoactive blend layer from pXL:CB = 80:20 (volume) rather than pXL alone, but the efficiency then decreased when the CB content increased further to pXL:CB = 60:40. The improved efficiency was correlated with a particular PTB7-Th:P(NDI2OD-T2) donor−acceptor blend nanostructure, evidenced by a fiber-like surface morphology, a red-shifted optical absorption, and enhanced PL quenching. Further device optimization for pXL:CB = 80:20 films yielded a power conversion efficiency of ~5.4%. However, these devices showed very poor stability (~15 min for a 50% reduction in initial efficiency), owing specifically to degradation of the PTB7-Th donor-component. Replacing PTB7-Th with a more stable donor polymer will be essential for any application potential to be realized.

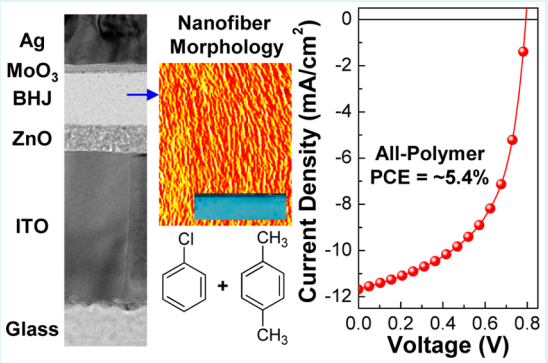

KEYWORDS: *polymer:polymer solar cells, cosolvents, nanostructure, stability, degradation*

INTRODUCTION

Polymer solar cells have attracted great attention for the past decade, due to their potential for rapid energy payback time and low-cost fabrication of flexible plastic solar modules.[1−5] The expectation for the low-cost fabrication can be attributed to the continuous roll-to-roll manufacturing by employing solution-coating processes at low temperatures and flexible thin film substrates made of plastic materials.[6−8] Since the early breakthroughs, most high efficiency (>8%) polymer solar cells have thus far been fabricated with the bulk heterojunction (BHJ) layers of electron-donating polymers and electron-accepting fullerenes, so-called polymer:fullerene solar cells.[9−25] However, the fullerene derivatives are small molecules, so that they have a tendency to recrystallize in the polymer:fullerene films, which is one of the crucial problems leading to the low stability of polymer:fullerene solar cells.[26−30]

Polymer:polymer solar cells, which have recently been called "all-polymer solar cells", have advantages over polymer:-fullerene solar cells because the electron-accepting components are polymers, instead of the fullerene derivatives, which can deliver better toughness than the small molecular fullerene derivatives in terms of chemical/morphological stability or durability due to easy tuning of chemical/electronic structure and entanglement of polymers.[4,31] Since the early works for polymer:polymer solar cells before 2005,[31−37] the power

Received: May 15, 2015
Accepted: July 1, 2015
Published: July 16, 2015

DOI: 10.1021/acsami.5b04224
ACS Appl. Mater. Interfaces 2015, 7, 15995−16002

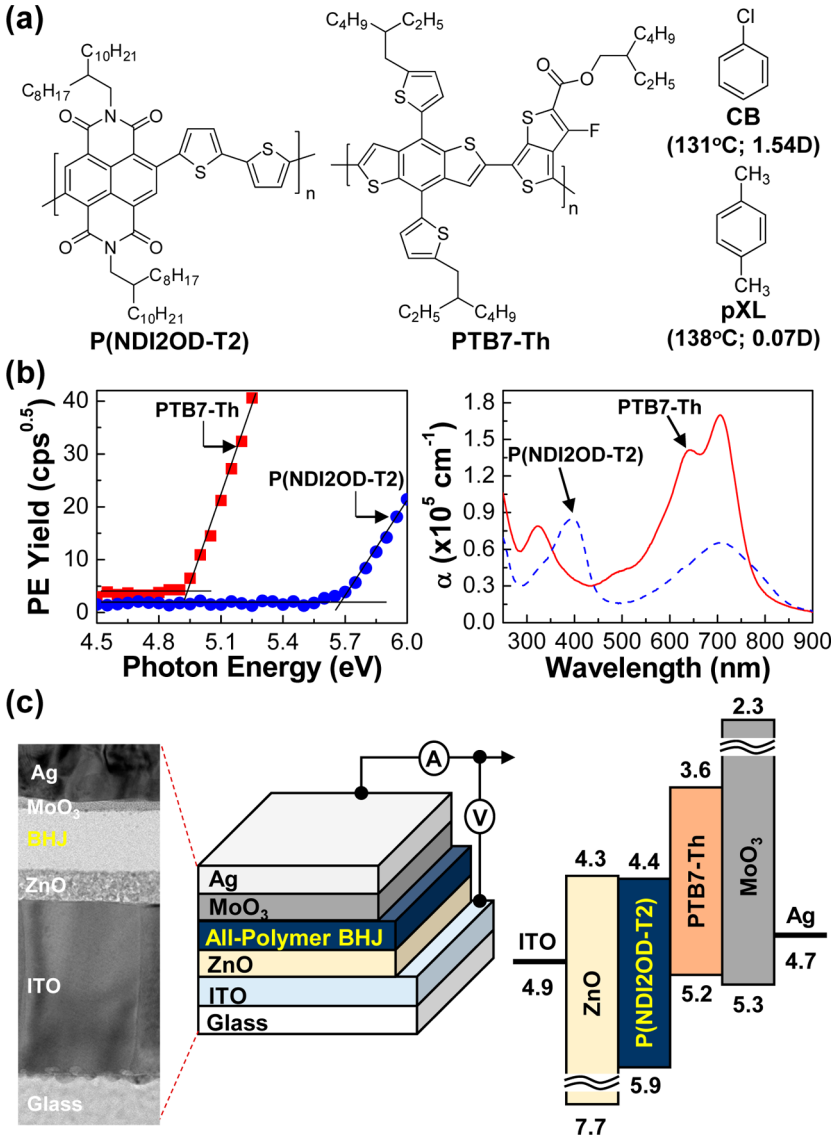

Figure 1. (a) Chemical structure of electron-donating (PTB7-Th) and electron-accepting (P(NDI2OD-T2) polymers and solvents (chlorobenzene and *p*-xylene). (b) Photoelectron (PE) yield spectra of the pristine PTB7-Th and P(NDI2OD-T2) films (layers). (c) Cross-sectional device structure and the flat energy band diagram for the present polymer:polymer solar cell (see the TEM image on the left): The thickness of each layer is given in the experimental section.

conversion efficiency (PCE) has been gradually improved by optimizing the nanostructure in the polymer:polymer BHJ layers and by using new polymer materials and solvent additives.[38−46] However, the efficiency of polymer:polymer solar cells is still far behind that of polymer:fullerene solar cells in spite of various approaches, including chemical doping and nanopatterning technology.

Very recently, Mori et al. reported 5.7% PCE for polymer:-polymer solar cells with the BHJ layers, which are composed of poly[4,8-bis(5-(2-ethylhexyl)thiophen-2-yl)benzo[1,2-b:4,5-b′]dithiophene-*alt*-3-fluorothieno[3,4-*b*]thiophene-2-carboxylate] (PTB7-Th) and poly[[*N*,*N*′-bis(2-octyldodecyl)-naphthalene-1,4,5,8-bis(dicarboximide)-2,6-diyl]-*alt*-5,5′-(2,2′-bithiophene)] (P(NDI2OD-T2)), by using chlorobenzene solvent and normal-type device structures.[45] In contrast, Fabiano et al. reported that using *p*-xylene rather than chlorobenzene is better for the improvement of efficiency due to the formation of lateral phase segregation for P(NDI2OD-T2).[47] In a similar period, we have also concentrated on the same material system and found that the quality of the polymer:polymer BHJ films prepared using *p*-xylene was quite dependent on the coating conditions, owing to the relatively low solubility of polymers in the *p*-xylene solvent, which led to the low reproduction ratio (probability) for achieving >5% PCE.

In this work, in order to overcome the low solubility problem by using *p*-xylene, we attempted to apply cosolvents of *p*-xylene (pXL) and chlorobenzene (CB) because chlorobenzene can compensate the low solubility problem of *p*-xylene. The composition of cosolvents was chosen as pXL:CB = 100:0, 80:20, and 60:40 by volume, which were used for the preparation of binary blend solutions of PTB7-Th and PI(NDI2OD-T2). The result showed that the efficiency of devices was quite sensitive to the composition of cosolvents. To understand the improved performances according to the cosolvents, the surface morphology and crystalline nanostructure of the PTB7-Th:P(NDI2OD-T2) BHJ layers was investigated using atomic force microscopy (AFM) and synchrotron-radiation grazing incidence X-ray diffraction

DOI: 10.1021/acsami.5b04224
ACS Appl. Mater. Interfaces 2015, 7, 15995−16002

(GIXD) measurements. Finally, the stability of the optimized devices (~5.4% PCE) was examined under continuous solar light illumination (100 mW/cm^2).

RESULTS AND DISCUSSION

The chemical structures of polymers and solvents are shown in Figure 1a. The dipole moment of solvents implies that chlorobenzene is more polar than *p*-xylene, which leads to the theory that chlorobenzene has better solvent power in dissolving the polymers with polar units in their main chains. The solubility test showed that a saturated solution could be achieved at 40 mg/mL (chlorobenzene) and 5 mg/mL (*p*-xylene) for PTB7-Th, while it could be made at 30 mg/mL (chlorobenzene) and 20 mg/mL (*p*-xylene) for P(NDI2OD-T2). Considering the boiling points of the two solvents, *p*-xylene is supposed to evaporate more slowly than chlorobenzene during a spin-coating process. Taking all these aspects into account, we fixed the cosolvent ratios of *p*-xylene (pXL) to chlorobenzene (CB) as pXL:CB = 100:0, 80:20, and 60:40 by volume, which have higher *p*-xylene concentrations in order to help better formation of lateral phase segregations in the resulting BHJ films.

First, we have rechecked the energy band structure of each polymer in a solid-state film to exactly understand the offset energy between PTB7-Th and P(NDI2OD-T2) in the BHJ films. As observed from the photoelectron (PE) yield spectra in Figure 1b (left), the difference of the ionization potential energy between PTB7-Th and P(NDI2OD-T2) was ca. 0.7 eV, which is sufficient to block the holes diffused from the PTB7-Th domain to the P(NDI2OD-T2) domain (we note that the highest occupied molecular orbital (HOMO) energy was finally obtained as 5.2 eV for PTB7-Th and 5.9 eV for P(NDI2OD-T2). The optical absorption spectra revealed that the absorption edge of P(NDI2OD-T2) was measured at a slightly longer wavelength than that of PTB7-Th (Figure 1b right and Figure S1), leading to the optical band gap energy of 1.5 eV for P(NDI2OD-T2) and 1.6 eV for PTB7-Th. As a consequence, the lowest unoccupied molecular orbital (LUMO) energy was calculated as 3.6 eV for PTB7-Th and 4.4 eV for P(NDI2OD-T2). Considering the large LUMO offset (0.8 eV) between PTB7-Th and P(NDI2OD-T2) in the case of solid-state films, the charge (electron) separation process is expected to occur efficiently from the excitons in the PTB7-Th domain to the LUMO level of the P(NDI2OD-T2) domain. In addition, the P(NDI2OD-T2) domain is considered to strongly contribute to the light harvesting when it comes to the optical absorption spectra in Figure 1b (right). On the basis of the energy band structure analysis for the two polymers in the solid state (Figure 1b), the inverted-type device structures were designed and fabricated (see the flat energy band structure for the full device in Figure 1c).

As shown in the current density–voltage (*J*–*V*) curves under a simulated solar light (air mass 1.5G, 100 mW/cm^2) (see Figure 2a), the short circuit current density (J_{SC}) of ca. 9.2 mA/cm^2 was measured for the polymer:polymer solar cell with the PTB7-Th:P(NDI2OD-T2) BHJ layer fabricated using *p*-xylene only (pXL:CB = 100:0). Interestingly, the J_{SC} value was noticeably increased up to ca. 11.7 mA/cm^2 for the polymer:polymer solar cell fabricated using the cosolvent of *p*-xylene and chlorobenzene (pXL:CB = 80:20). In addition, the fill factor (FF) was also increased from ca. 49.7% to 54% when the solvent was changed from *p*-xylene to the cosolvent (pXL:CB = 80:20). Here it is noticeable that the open circuit voltage (V_{OC}) was very marginally decreased by 0.01 V (from 0.799 to 0.789 V) by using the cosolvent (pXL:CB = 80:20). As a result, the power conversion efficiency was improved up to 5% from 3.6% by using the cosolvent (pXL:CB = 80:20). However, when the concentration of chlorobenzene was increased (pXL:CB = 60:40), both J_{SC} and V_{OC} were remarkably decreased, except the FF value, from those in the case of using *p*-xylene only. This result indicates that the device performance became worse when the chlorobenzene content increased, owing to the poor formation of lateral phase segregation as reported in ref 47 (see Table S1 for the summary of averaged device performances with more than 10 devices).

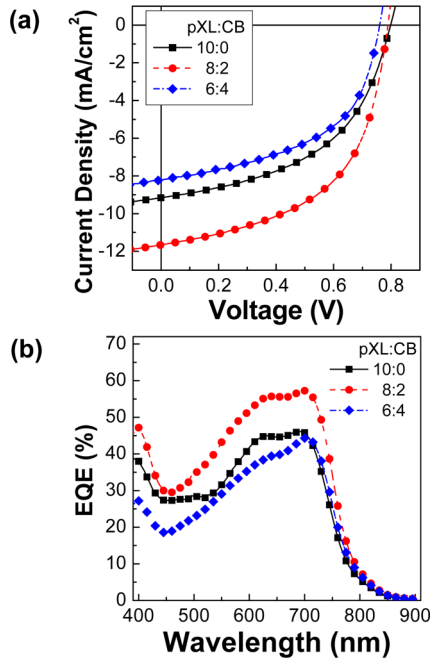

Figure 2. (a) Light current density–voltage (*J*–*V*) curves under illumination of a simulated solar light (air mass 1.5 G, 100 mW/cm^2). (b) EQE spectra for polymer:polymer solar cells fabricated with the PTB7-Th:P(NDI2OD-T2) BHJ layers according to the composition of cosolvents (pXL:CB).

As shown in the external quantum efficiency (EQE) spectra (see Figure 2b), the photocurrent signal was clearly measured up to 850 nm for all devices, which is attributed to the contribution of both polymers when it comes to the optical absorption spectra in Figure 2b. In terms of EQE values, a similar trend as obtained for the light *J*–*V* curves was measured for the EQE spectra according to the cosolvent compositions. In other words, the EQE value was higher for the polymer:polymer solar cell fabricated using the cosolvent (pXL:CB = 80:20) than that using the *p*-xylene (pXL:CB = 100:0) over the entire wavelength measured in this work. Here we note that the spectral shape is almost identical for the cosolvent (pXL:CB = 80:20) case and the *p*-xylene (pXL:CB = 100:0) case. However, the cosolvent (pXL:CB = 60:40) resulted in a slightly different spectral shape compared to other cases, which may reflect the formation of different nanostructures in the BHJ layers (films) according to the cosolvent compositions.

To examine the nanostructures in the BHJ layers according to the compositions of cosolvent, we first measured the optical absorption and photoluminescence (PL) spectra for the BHJ layers. As shown in Figure 3a, the optical absorption spectrum of the BHJ layers was slightly red-shifted as the chlorobenzene

DOI: 10.1021/acsami.5b04224
ACS Appl. Mater. Interfaces 2015, 7, 15995–16002

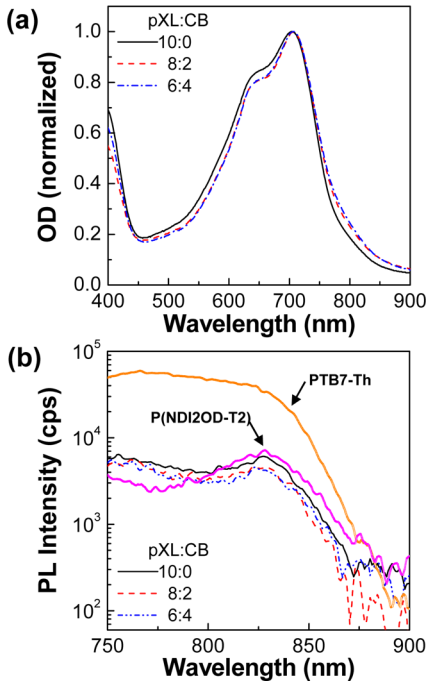

Figure 3. (a) Normalized optical density (OD) spectra of the PTB7-Th:P(NDI2OD-T2) BHJ layers. (b) Photoluminescence (PL) spectra of the pristine polymer (PTB7-Th and P(NDI2OD-T2)) films (layers) and the PTB7-Th:P(NDI2OD-T2) BHJ layers according to the composition of cosolvents.

content increased. This result may reflect that the chain stacking of polymers in the BHJ layers is dependent on the composition of cosolvent. The PL intensity of the BHJ layers was noticeably decreased compared to that of the pristine layers (note that the PL quenching was more pronounced from the PTB7-Th layer than from the P(NDI2OD-T2) layer) (see Figure 3b and Figure S2a). This result supports that the charge separation between PTB7-Th and P(NDI2OD-T2) is quite efficient in the PTB7-Th:P(NDI2OD-T2) BHJ layers. Interestingly, the PL intensity was relatively lower for the BHJ layer prepared using the cosolvents than that prepared using *p*-xylene only (see also Figure S2b), which informs us of better charge separation in the case of using cosolvents. However, we recall that the cosolvent (pXL:CB = 60:40) resulted in relatively poor solar cell performances compared to the *p*-xylene solvent (see Figure 2), which is in disagreement with the PL quenching result. Therefore, it is considered that the cosolvent (pXL:CB = 60:40) induced too intimate mixing between the two polymer components, leading to the increased charge blocking resistances in the BHJ layers (see Table S1 for the slightly increased series resistance (R_S = 0.22 kΩ·cm^2) for the 60:40 composition compared to R_S = 0.17 kΩ·cm^2 for the 80:20 composition).[36]

Next, the surface nanostructure of the PTB7-Th:P(NDI2OD-T2) BHJ layers, which were coated on the ZnO-coated ITO-glass substrates, was investigated with atomic force microscopy (AFM). As shown in Figure 4, the surface of the BHJ layers prepared using the cosolvent (pXL:CB = 80:20) exhibited a particular nanofiber-like morphology, which is certainly different from the random surfaces in the BHJ layer prepared using *p*-xylene only. Considering the formation of a nanofiber-like morphology in the pristine P(NDI2OD-T2) film (layer) as reported by Tremel et al.,[48] the P(NDI2OD-T2)

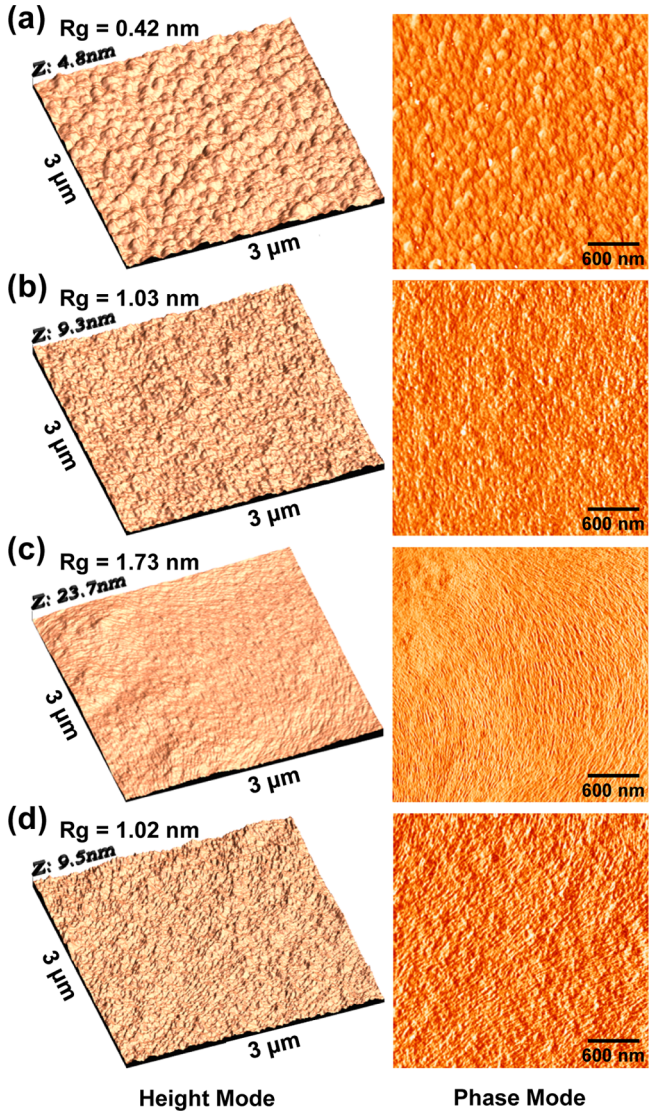

Figure 4. 3D height mode (left) and 2D phase mode (right) AFM images: (a) ZnO layer and (b–d) PTB7-Th:P(NDI2OD-T2) BHJ layers coated on the ZnO layers prepared using cosolvents (pXL:CB = 100:0) (b), (80:20) (c), and (60:40) (d). "Rg" denotes the surface roughness.

component might be enriched on the surface of the BHJ layers when the cosolvent (pXL:CB = 80:20) was used. However, the surface morphology of the BHJ layers became random again in the presence of very slight traces of nanofiber-like structures when the CB composition in the cosolvent was increased (pXL:CB = 60:40). It is noteworthy that the surface roughness of the BHJ layer prepared using the cosolvent (pXL:CB = 80:20) was higher than that of the other two BHJ layers prepared using either *p*-xylene or the cosolvent (pXL:CB = 60:40) even though there are many well-aligned nanofiber-like fine patterns on the surface of the BHJ layer prepared using the cosolvent (pXL:CB = 80:20). Hence the relatively better device performance at pXL:CB = 80:20 might be closely related to the higher surface roughness with the well-aligned nanofiber-like morphology at this solvent composition.

Based on the information on the surface morphology for the BHJ layers according to the composition of cosolvents, the crystalline nanostructure of the BHJ layers was further investigated by employing a synchrotron GIXD technique

DOI: 10.1021/acsami.5b04224
ACS Appl. Mater. Interfaces 2015, 7, 15995−16002

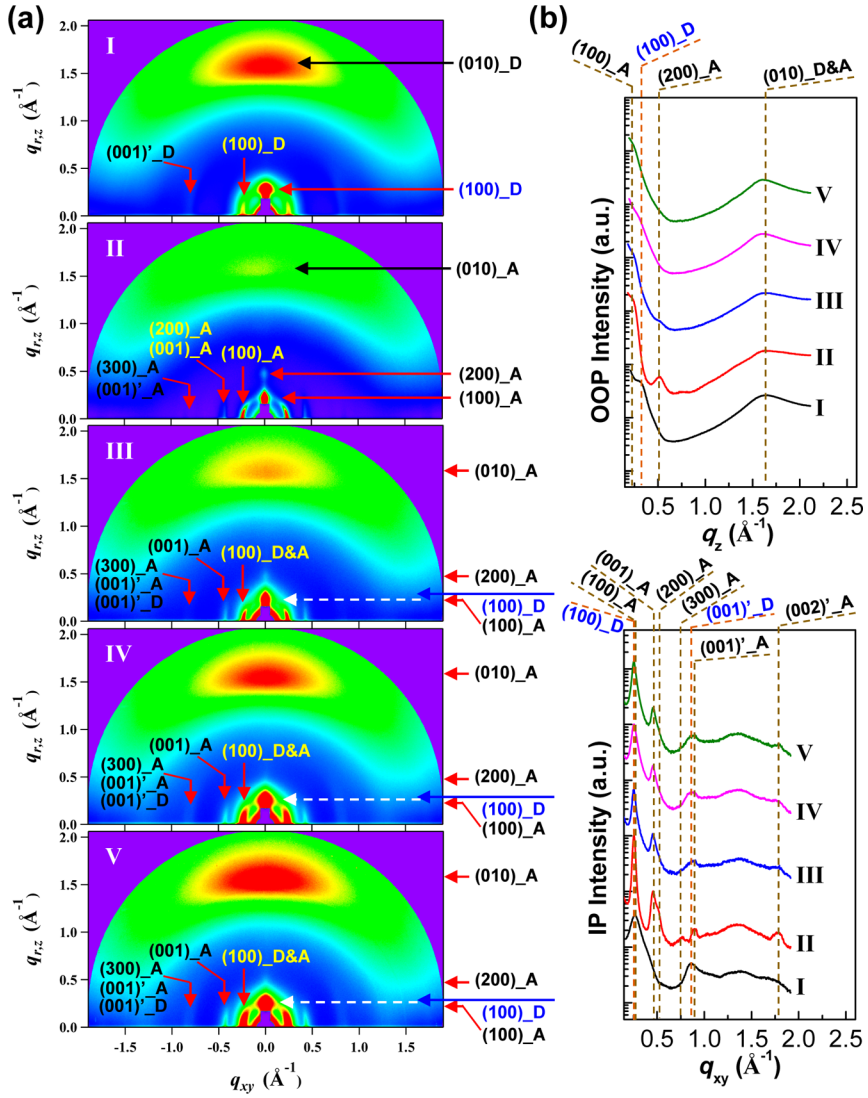

Figure 5. (a) 2D GIXD images and (b) 1D GIXD profiles for the pristine polymer layers (I: PTB7-Th and II: P(NDI2OD-T2)) and the BHJ layers prepared using cosolvents (III: 100:0, IV: 80:20, V: 60:40). Note that the major diffraction peaks for each polymer are marked on the 2D images and on the top part of the 1D graphs. The labels "D" and "A" in the assigned diffraction peaks stand for "PTB7-Th" and "P(NDI2OD-T2)", respectively.

(see the limitations and advantages of GIXD techniques in ref 49). As shown in Figure 5a, a dominant face-on chain stacking structure was measured for the pristine PTB7-Th layer and the pristine P(NDI2OD-T2) layer which were coated on the ZnO-coated ITO-glass substrates.[44] The exact diffraction position for each polymer is clearly observed from the 1D GIXD profiles in Figure 5b (see the detailed analysis data including *d*-spacing for the GIXD profiles in Table. S2). The (100) peak of the pristine P(NDI2OD-T2) layer was measured at a smaller angle (diffraction vector), as clearly observed in the out-of-plane (OOP) direction, and was relatively narrower in the peak width (i.e., smaller full width at half-maximum) compared to that of the pristine PTB7-Th layer in the in-plane (IP) direction. For the BHJ layers, interestingly, the diffraction spots by the PTB7-Th component (see (100)_D and (010)_D in Figure 5a III) were considerably weakened in the case of *p*-xylene solvent (pXL:CB = 100:0) even though those by the P(NDI2OD-T2) component were well maintained. However, in the case of cosolvents, all diffraction spots by both components were well kept in the 2D GIXD images (see Figure 5a IV and V). This result implies that the chain stacking of the PTB7-Th component in the BHJ layer was relatively more prevented by the presence of the P(NDI2OD-T2) component when *p*-xylene was used only. The weakened diffraction of the PTB7-Th component in the case of using *p*-xylene is also evidenced from the 1D GIXD profiles in the IP direction because the (001)'_A peak of the P(NDI2OD-T2) component was pronounced but the (001)'_D peak of the PTB7-Th component was almost not observed in the BHJ layer. Thus, the retarded crystallization of the PTB7-Th component in the BHJ layer prepared using *p*-xylene only can be attributed to the relatively inferior solar cell performances compared to the cosolvent (pXL:CB = 80:20). In addition, a close look at the 1D GIXD profiles in the IP direction delivers that the (001)'_D peak is slightly (marginally) less pronounced in the case of the cosolvent (pXL:CB = 60:40) than the cosolvent (pXL:CB = 80:20), which might be one of the clues for the relatively low solar cell performances, together with the obviously different surface morphology (see Figure 4), in the case of using the cosolvent (pXL:CB = 60:40).

Finally, the device optimization was performed for the solar cells with the PTB7-Th:P(NDI2OD-T2) BHJ layers prepared

DOI: 10.1021/acsami.5b04224
ACS Appl. Mater. Interfaces 2015, 7, 15995−16002

using the cosolvent (pXL:CB = 80:20), and the optimized devices were subject to the examination of stability (lifetime). As shown in Figure 6a, the optimized polymer:polymer solar

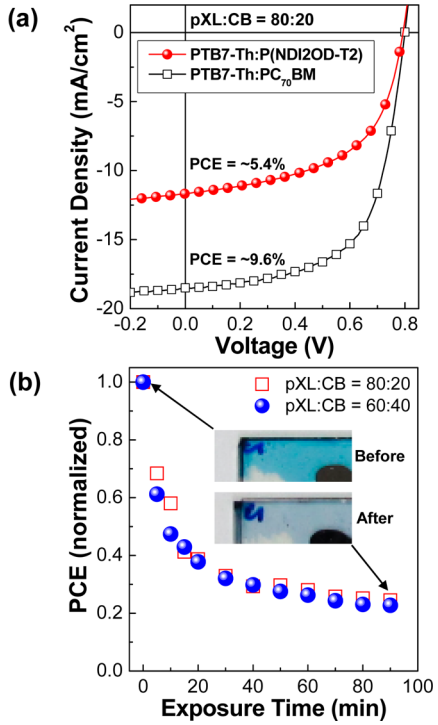

Figure 6. (a) Light J–V curves under illumination of a simulated solar light (air mass 1.5G, 100 mW/cm^2) for the optimized polymer:-polymer solar cell (PTB7-Th:P(NDI2OD-T2)) (J_{SC} = 12 mA/cm^2, V_{OC} = 0.80 V, FF = 56%) and the control device (PTB7-Th:PC$_{70}$BM) (J_{SC} = 17 mA/cm^2, V_{OC} = 0.77 V, FF = 73%). (b) Normalized PCE of polymer:polymer solar cells as a function of exposure time under continuous illumination of a simulated solar light (air mass 1.5G, 100 mW/cm^2) according to the composition of cosolvents (pXL:CB = 80:20 and pXL:CB = 60:40): The inset photographs show the color of the BHJ layer before and after illumination (90 min).

cell with the PTB7-Th:P(NDI2OD-T2) BHJ layer exhibited ca. 5.4% PCE, which is considered one of the highest efficiencies (>5%) so far for polymer:polymer solar cells (see Table S3 for the recent progress in polymer:polymer solar cells). Note that the optimized polymer:polymer solar cell with 5.4% PCE was fabricated and measured at the same time/condition as done for the (control) PTB7-Th:PC70BM solar cell that is certified to deliver ca. 9.5% PCE (see Figure S3).

The 5.4% PCE device, which was mounted inside an argon-filled sample holder in order to avoid any moisture and oxygen effects, was subject to the stability test under continuous solar light illumination (100 mW/cm^2). As shown in Figure 6b, the efficiency was quickly decreased and reached half the initial value at the exposure time of less than 15 min. After ca. 30 min the efficiency decay rate became slow and then the efficiency at 90 min became approximately 25% of the initial value (see other solar cell parameters in Figure S4). Interestingly, the decay trend of the optimized device was quite similar to that of the device with the BHJ layer prepared using the cosolvent (pXL:CB = 60:40). This result implies that the striking efficiency decrease can be ascribed mainly to the degradation of the polymer materials, as previously reported for the PTB7 material in the polymer:fullerene solar cells.[9] As shown in the inset photographs in Figure 6b, the color of the PTB7-Th:P(NDI2OD-T2) BHJ layer was noticeably changed after 90 min of illumination. To understand which component between PTB7-Th and P(NDI2OD-T2) is mainly responsible for the color change (efficiency decrease), the optical absorption and PL spectra were measured before and after continuous solar light illumination (90 min) for the pristine polymer layers and the BHJ layers. As shown in Figure S5, the optical absorption coefficient (α) of the pristine PTB7-Th layer was remarkably decreased after 90 min of illumination (see the wavelength ranges between 600 and 900 nm), whereas that of the pristine P(NDI2OD-T2) layer was almost little changed. In addition, the PL intensity reduction was extremely huge by more than 10-fold for the pristine PTB7-Th layer, whereas it was quite marginal, as low as ca.1.4-fold for the pristine P(NDI2OD-T2) layer. The optical absorption coefficient in the BHJ layers was also greatly reduced after 90 min illumination, irrespective of the composition of cosolvents (see Figure S6), which can be obviously attributed to the degradation of the PTB7-Th component. Here we note that the reduction in the PL intensity for the BHJ layers was not pronounced because of the already largely lowered PL intensity by the charge separation between the two components.

CONCLUSIONS

The effect of cosolvents, which are composed of *p*-xylene (pXL) and chlorobenzene (CB), was investigated for polymer:-polymer solar cells with the PTB7-Th:P(NDI2OD-T2) BHJ layers. The performance of polymer:polymer solar cells was considerably improved when the cosolvent (pXL:CB = 80:20) was used for the preparation of blend solutions. However, when the CB content was increased up to 40 vol % (pXL:CB = 60:40), the solar cell performance became poor again. The improved performance by using the cosolvent (pXL:CB = 80:20) was explained by both the red-shifted optical absorption spectra and the better PL quenching (charge separation), while it was also attributed to the formation of the particular nanofiber-like surface morphology that is closely related to the crystalline nanostructure change as measured by the synchrotron GIXD measurement. The optimized device fabricated using the cosolvent (pXL:CB = 80:20) exhibited ~5.4% PCE. The stability test showed that the lifetime of the optimized device was very poor (half-life = ~15 min), which was attributed to the degradation of the PTB7-Th component as proven by the optical characterization for both the pristine layers and the BHJ layers.

METHODS

Materials and Solutions. PTB7-Th (weight-average molecular weight =126 kDa and polydispersity index = 2.5) and P(NDI2OD-T2) (weight-average molecular weight = 25–50 kDa and polydispersity index = 1.5–3.5) were received from 1-Material (Canada) and Polyera, respectively. Zinc acetate dehydrate (purity> 99%) was purchased from Sigma-Aldrich (United States) and used without further purification. The binary polymer blend solutions were prepared using the cosolvents of *p*-xylene and chlorobenzene (pXL:CB = 10:0, 8:2, 6:4 by volume) at a solid concentration of 10 mg/mL (PTB7Th:P(NDI2OD-T2) = 1:1 by weight), followed by stirring at room temperature for 12 h prior to spin-coating. The ZnO precursor solutions were prepared by dissolving zinc acetate dehydrate (1 g) in the mixture of 2-methoxyethanol (10 mL) and ethanolamine (0.28 mL as stabilizer), which were stirred at 60 °C for 3 h and then at room temperature for 12 h before spin-coating.

DOI: 10.1021/acsami.5b04224
ACS Appl. Mater. Interfaces 2015, 7, 15995–16002

Thin film and Device Fabrication. The patterned ITO-coated glass substrates (12 Ω/cm^2, Asahi/AMG) were cleaned using acetone and isopropyl alcohol inside an ultrasonic cleaner. The wet-cleaned ITO-glass substrates were dried with a nitrogen flow and treated inside a UV-ozone system (AH-1700, Ahtech LTS) for 20 min in order to remove any remnant organic residue on the surface of the substrates. Next, the ZnO precursor solutions were spun on the ITO-glass substrates and the resulting ZnO nanolayers (thickness = 30 nm) were baked at 200 °C for 1 h in air ambient condition (laboratory atmosphere). Then the BHJ layers were spin-coated on the top of the ZnO nanolayers in a nitrogen-filled glovebox and dried inside the same glovebox. After transferring all the samples to a vacuum chamber, MoO_3 (10 nm) and Ag (80 nm) were thermally evaporated on the top of the BHJ layers. The area of the active zones in the fabricated devices was 0.05 cm^2. For the optical measurements the film samples were prepared by spin-coating on quartz substrates, whereas the samples for AFM and GIXD measurements were prepared in the same way as for the device fabrication.

Device Measurements. The film thickness was measured using a surface profiler (Alpha Step 20, Tencor Instruments). The optical absorption and photoluminescence (PL) spectra were measured using a UV−visible spectrometer (Optizen 2120, MECASYS) and a PL spectrometer (FS-2, SCINCO), respectively. The HOMO energy level of the pristine films was measured using a photoelectron yield spectrometer (AC2, Riken-Keiki). The surface morphology of the BHJ layers was measured using an atomic force microscope (AFM, Nanoscope IIIa, Digital Instruments). The nanostructure of the BHJ layers was measured using a synchrotron radiation-grazing incidence X-ray diffraction (GIXD) system (X-ray wavelength = 0.112 nm, incidence angle = 0.125°, 9A, U-SAXS beamline, Pohang Accelerator Laboratory) and a field-emission transmission electron microscope (FE-TEM, Titan G2 ChemiSTEM Cs Probe, FEI Company). The current density−voltage (J−V) curves of solar cells were obtained using a solar cell measurement system equipped with a solar simulator (92250A-1000, Newport-Oriel) and an electrometer (Keithley 2400). The EQE measurement of devices was carried out using a specialized measurement system equipped with a light source (Tungsten-Halogen lamp, 150W, ASBN-W, Spectral Products), a monochromator (CM110, Spectra Products) and a calibrated (certified) Si-photodiode. All devices were measured under an inert environment using an argon-filled sample holder. The series resistance (R_S) was calculated from the slope in the light J−V curves at open circuit condition (0 mA/cm^2), while the shunt resistance (R_{SH}) was obtained from the slope in the light J−V curves at short circuit condition (0 V).

■ ASSOCIATED CONTENT

Supporting Information

Summary of solar cell performances, summary of GIXD parameters, summary of recent reports on high PCE polymer:-polymer solar cells, enlarged absorption spectra at the absorption edge, PL spectra, accreditation results for the control device, stability test results, and absorption and PL spectra before and after 90 min illumination. The Supporting Information is available free of charge on the ACS Publications website at DOI: 10.1021/acsami.5b04224.

■ AUTHOR INFORMATION

Corresponding Authors

*E-mail: khj217@knu.ac.kr.

*E-mail: ykimm@knu.ac.kr. Tel: +82-53-950-5616.

Notes

The authors declare no competing financial interest.

■ ACKNOWLEDGMENTS

This work was financially supported by grants from Korean Government (NRF_2015R1A2A2A01003743, Basic Research Laboratory Program_2011-0020264, Basic Science Research Program_2009-0093819, NRF_2014R1A1A3051165, Human Resource Training Project for Regional Innovation_-MOE(NRF_2014H1C1A1066748), and NRF_2014R1A6A3A03055861). This work was also partly supported by the DGIST R&D Program of the Ministry of Science, ICT and Future Planning of Korea (15-EN-03). All experiments at PLS were supported in part by MSIP and POSTECH.

■ REFERENCES

(1) Wu, J.-S.; Cheng, S.-W.; Cheng, Y.-J.; Hsu, C.-S. Donor-Acceptor Conjugated Polymers Based on Multifused Ladder-Type Aenes for Organic Solar Cells. *Chem. Soc. Rev.* **2015**, *44*, 1113−1154.

(2) Lu, L.; Yu, L. Understanding Low Bandgap Polymer PTB7 and Optimizing Polymer Solar Cells Based on It. *Adv. Mater.* **2014**, *26*, 4413−4430.

(3) You, J.; Dou, L.; Hong, Z.; Li, G.; Yang, Y. Recent Trends in Polymer Tandem Solar Cells Research. *Prog. Polym. Sci.* **2013**, *38*, 1909−1928.

(4) Facchetti, A. Polymer Donor−Polymer Acceptor (All-Polymer) Solar Cells. *Mater. Today* **2013**, *16*, 123−132.

(5) Darling, S. B.; You, F. The Case for Organic Photovoltaics. *RSC Adv.* **2013**, *3*, 17633−17648.

(6) Søndergaard, R.; Hösel, M.; Krebs, F. C. Roll-to-Roll Fabrication of Lrge Area Functional Organic Materials. *J. Polym. Sci., Part B: Polym. Phys.* **2013**, *51*, 16−34.

(7) Yu, J.-S.; Kim, I.; Kim, J.-S.; Jo, J.; Larsen-Olsen, T. T.; Søndergaard, R. R.; Hösel, M.; Angmo, D.; Jørgensen, M.; Krebs, F. C. Silver Front Electrode Grids for ITO-Free All Printed Polymer Solar Cells with Embedded and Raised Topographies, Prepared by Thermal Imprint, Flexographic and Inkjet Roll-to-Roll Processes. *Nanoscale* **2012**, *4*, 6032−6040.

(8) Voigt, M. M.; Mackenzie, R. C. I.; Yau, C. P.; Atienzar, P.; Dane, J.; Keivanidis, P. E.; Bradley, D. D. C.; Nelson, J. Gravure Printing for Three Subsequent Solar Cell Layers of Inverted Structures on Flexible Substrates. *Sol. Energy Mater. Sol. Cells* **2011**, *95*, 731−734.

(9) Woo, S.; Kim, W. H.; Kim, H.; Yi, Y.; Lyu, H.-K.; Kim, Y. 8.9% Single-Stack Inverted Polymer Solar Cells with Electron-Rich Polymer Nanolayer-Modified Inorganic Electron-Collecting Buffer Layers. *Adv. Energy Mater.* **2014**, DOI: 10.1002/aenm.201301692.

(10) Nguyen, T. L.; Choi, H.; Ko, S.-J.; Uddin, M. A.; Walker, B.; Yum, S.; Jeong, J.-E.; Yun, M. H.; Shin, T. J.; Hwang, S.; Kim, J. Y.; Woo, H. Y. Semi-crystalline Photovoltaic Polymers with Efficiency Exceeding 9% in a ~300 nm Thick Conventional Single-Cell Device. *Energy Environ. Sci.* **2014**, *7*, 3040−3051.

(11) Guo, X.; Zhou, N.; Lou, S. J.; Smith, J.; Tice, D. B.; Hennek, J. W.; Ortiz, R. P.; Navarrete, J. T. L.; Li, S.; Strzalka, J.; Chen, L. X.; Chang, R. P. H.; Facchetti, A.; Marks, T. J. Polymer Solar Cells with Enhanced Fill Factors. *Nat. Photonics* **2013**, *7*, 825−833.

(12) Li, W.; Furlan, A.; Hendriks, K. H.; Wienk, M. M.; Janssen, R. A. J. Efficient Tandem and Triple-Junction Polymer Solar Cells. *J. Am. Chem. Soc.* **2013**, *135*, 5529−5532.

(13) Liao, S.-H.; Jhuo, H.-J.; Cheng, Y.-S.; Chen, S.-A. Fullerene Derivative-Doped Zinc Oxide Nanofilm as the Cathode of Inverted Polymer Solar Cells with Low-Bandgap Polymer (PTB7-Th) for High Performance. *Adv. Mater.* **2013**, *25*, 4766−4771.

(14) Zhang, M.; Gu, Y.; Guo, X.; Liu, F.; Zhang, S.; Huo, L.; Russell, T. P.; Hou, J. Efficient Polymer Solar Cells Based on Benzothiadiazole and Alkylphenyl Substituted Benzodithiophene with a Power Conversion Efficiency over 8%. *Adv. Mater.* **2013**, *25*, 4944−4949.

(15) You, J.; Chen, C.-C.; Hong, Z.; Yoshimura, K.; Ohya, K.; Xu, R.; Ye, S.; Gao, J.; Li, G.; Yang, Y. 10.2% Power Conversion Efficiency Polymer Tandem Solar Cells Consisting of Two Identical Sub-Cells. *Adv. Mater.* **2013**, *25*, 3973−3978.

(16) Deng, Y.; Liu, J.; Wang, J.; Liu, L.; Li, W.; Tian, H.; Zhang, X.; Xie, Z.; Geng, Y.; Wang, F. Dithienocarbazole and Isoindigo Based Amorphous Low Bandgap Conjugated Polymers for Efficient Polymer Solar Cells. *Adv. Mater.* **2014**, *26*, 471−476.

DOI: 10.1021/acsami.5b04224
ACS Appl. Mater. Interfaces 2015, 7, 15995−16002

(17) Wang, N.; Chen, Z.; Wei, W.; Jiang, Z. Fluorinated Benzothiadiazole-Based Conjugated Polymers for High-Performance Polymer Solar Cells without Any Processing Additives or Post-Treatments. *J. Am. Chem. Soc.* **2013**, *135*, 17060−17068.
(18) Cabanetos, C.; El Labban, A.; Bartelt, J. A.; Douglas, J. D.; Mateker, W. R.; Fréchet, J. M. J.; McGehee, M. D.; Beaujuge, P. M. Linear Side Chains in Benzo[1,2-b:4,5-b′]dithiophene-thieno[3,4-c]pyrrole-4,6-dione Polymers Direct Self-Assembly and Solar Cell Performance. *J. Am. Chem. Soc.* **2013**, *135*, 4656−4659.
(19) Liu, Y.; Zhao, J.; Li, Z.; Mu, C.; Ma, W.; Hu, H.; Jiang, K.; Lin, H.; Ade, H.; Yan, H. Aggregation and Morphology Control Enables Multiple Cases of High-Efficiency Polymer Solar Cells. *Nat. Commun.* **2014**, *5*, 5293.
(20) Shaheen, S. E.; Brabec, C. J.; Sariciftci, N. S.; Padinger, F.; Fromherz, T.; Hummelen, J. C. 2.5% Efficient Organic Plastic Solar Cells. *Appl. Phys. Lett.* **2001**, *78*, 841−843.
(21) Padinger, F.; Rittberger, R. S.; Sariciftci, N. S. Effects of Postproduction Treatment on Plastic Solar Cells. *Adv. Funct. Mater.* **2003**, *13*, 85−88.
(22) Kim, Y.; Choulis, S. A.; Nelson, J.; Bradley, D. D. C.; Cook, S.; Durrant, J. R. Device Annealing Effect in Organic Solar Cells with Blends of Regioregular Poly(3-hexylthiophene) and Soluble Fullerene. *Appl. Phys. Lett.* **2005**, *86*, 063502.
(23) Reyes-Reyes, M.; Kim, K.; Carroll, D. L. High-Efficiency Photovoltaic Devices Based on Annealed Poly(3-hexylthiophene) and 1-(3-methoxycarbonyl)-propyl-1-phenyl-(6,6)C_{61} Blends. *Appl. Phys. Lett.* **2005**, *87*, 083506.
(24) Li, G.; Shrotriya, V.; Huang, J.; Yao, Y.; Moriarty, T.; Emery, K.; Yang, Y. High-Efficiency Solution Processable Polymer Photovoltaic Cells by Self-Organization of Polymer Blends. *Nat. Mater.* **2005**, *4*, 864−868.
(25) Kim, Y.; Cook, S.; Tuladhar, S. M.; Choulis, S. A.; Nelson, J.; Durrant, J. R.; Bradley, D. D. C.; Giles, M.; McCulloch, I.; Ha, C.-S.; Ree, M. A Strong Regioregularity Effect in Self-Organizing Conjugated Polymer Films and High-Efficiency Polythiophene:Fullerene Solar Cells. *Nat. Mater.* **2006**, *5*, 197−203.
(26) Yang, X.; Loos, J.; Veenstra, S. C.; Verhees, W. J. H.; Wienk, M. M.; Kroon, J. M.; Michels, M. A. J.; Janssen, R. A. J. Nanoscale Morphology of High-Performance Polymer Solar Cells. *Nano Lett.* **2005**, *5*, 579−583.
(27) Kim, Y.; Nelson, J.; Zhang, T.; Cook, S.; Durrant, J. R.; Kim, H.; Park, J.; Shin, M.; Nam, S.; Heeney, M.; McCulloch, I.; Ha, C.-S; Bradley, D. D. C. Distorted Asymmetric Cubic Nanostructure of Soluble Fullerene Crystals in Efficient Polymer:Fullerene Solar Cells. *ACS Nano* **2009**, *3*, 2557−2562.
(28) Kim, H.; Shin, M.; Park, J.; Kim, Y. Effect of Long Time Annealing and Incident Light Intensity on the Performance of Polymer:Fullerene Solar Cells. *IEEE Trans. Nanotechnol.* **2010**, *9*, 400−406.
(29) Kim, H.; Shin, M.; Park, J.; Kim, Y. Initial Performance Changes of Polymer/Fullerene Solar Cells by Short-Time Exposure to Simulated Solar Light. *ChemSusChem* **2010**, *3*, 476−480.
(30) Wong, H. C.; Li, Z.; Tan, C. H.; Zhong, H.; Huang, Z.; Bronstein, H.; McCulloch, I.; Cabral, J. T.; Durrant, J. R. Morphological Stability and Performance of Polymer-Fullerene Solar Cells under Thermal Stress - the Impact of Photo-Induced $PC_{60}BM$ Oligomerisation. *ACS Nano* **2014**, *8*, 1297−1308.
(31) Kim, Y.; Cook, S.; Choulis, S. A.; Nelson, J.; Durrant, J. R.; Bradley, D. D. C. Organic Photovoltaic Devices Based on Blends of Regioregular Poly (3-hexylthiophene) and Poly (9,9-dioctylfluorene-co-benzothiadiazole). *Chem. Mater.* **2004**, *16*, 4812−4818.
(32) Yu, G.; Heeger, A. J. Charge Separation and Photovoltaic Conversion in Polymer Composites with Internal Donor/Acceptor Heterojunctions. *J. Appl. Phys.* **1995**, *78*, 4510−4515.
(33) Friend, R. H.; Granström, M.; Petritsch, K.; Arias, A. C.; Lux, A.; Andersson, M. R. Laminated Fabrication of Polymeric Photovoltaic Diodes. *Nature* **1998**, *395*, 257−260.
(34) Arias, A. C.; MacKenzie, J. D.; Stevenson, R.; Halls, J. J.M.; Inbasekaran, M.; Woo, E. P.; Richards, D.; Friend, R. H. Photovoltaic Performance and Morphology of Polyfluorene Blends: A Combined Microscopic and Photovoltaic Investigation. *Macromolecules* **2001**, *34*, 6005−6013.
(35) Alam, M. M.; Jenekhe, S. A. Efficient Solar Cells from Layered Nanostructures of Donor and Acceptor Conjugated Polymers. *Chem. Mater.* **2004**, *16*, 4647−4656.
(36) Halls, J. J. M.; Walsh, C. A.; Greenham, N. C.; Marseglia, E. A.; Friend, R. H.; Moratti, S. C.; Holmes, A. B. Efficient Photodiodes from Interpenetrating Polymer Networks. *Nature* **1995**, *376*, 498−500.
(37) Kietzke, T.; Hörhold, H.-H.; Neher, D. Efficient Polymer Solar Cells Based on M3EH−PPV. *Chem. Mater.* **2005**, *17*, 6532−6537.
(38) McNeill, C. R.; Abrusci, A.; Zaumseil, J.; Wilson, R.; McKiernan, M. J.; Burroughes, J. H.; Halls, J. J. M.; Greenham, N. C.; Friend, R. H. Dual Electron Donor/Electron Acceptor Character of a Conjugated Polymer in Efficient Photovoltaic diodes. *Appl. Phys. Lett.* **2007**, *90*, 193506.
(39) Mori, D.; Benten, H.; Kosaka, J.; Ohkita, H.; Ito, S.; Miyake, K. Polymer/Polymer Blend Solar Cells with 2.0% Efficiency Developed by Thermal Purification of Nanoscale-Phase-Separated Morphology. *ACS Appl. Mater. Interfaces* **2011**, *3*, 2924−2927.
(40) Holcombe, T. W.; Woo, C. H.; Kavulak, D. F. J.; Thompson, B. C.; Fréchet, J. M. J. All-Polymer Photovoltaic Devices of Poly(3-(4-n-octyl)-phenylthiophene) from Grignard Metathesis (GRIM) Polymerization. *J. Am. Chem. Soc.* **2009**, *131*, 14160−14161.
(41) Nam, S.; Shin, M.; Kim, H.; Ha, C.-S.; Ree, M.; Kim, Y. Improved Performance of Polymer:Polymer Solar Cells by Doping Electron-Accepting Polymers with an Organosulfonic Acid. *Adv. Funct. Mater.* **2011**, *21*, 4527−4534.
(42) Liu, X.; Huettner, S.; Rong, Z.; Sommer, M.; Friend, R. H. Solvent Additive Control of Morphology and Crystallization in Semiconducting Polymer Blends. *Adv. Mater.* **2012**, *24*, 669−674.
(43) Facchetti, A. Presented at the 3rd Conference on Organic Photovoltaics, Würzburg, Germany, 2012, http://faculty.wcas.northwestern.edu/~afa912/.
(44) Kang, H.; Kim, K.-H.; Choi, J.; Lee, C.; Kim, B. J. High-Performance All-Polymer Solar Cells Based on Face-On Stacked Polymer Blends with Low Interfacial Tension. *ACS Macro Lett.* **2014**, *3*, 1009−1014.
(45) Mori, D.; Benten, H.; Okada, I.; Ohkita, H.; Ito, S. Highly Efficient Charge-Carrier Generation and Collection in Polymer/Polymer Blend Solar Cells with a Power Conversion Efficiency of 5.7%. *Energy Environ. Sci.* **2014**, *7*, 2939−2943.
(46) Liao, H.-C.; Ho, C.-C.; Chang, C.-Y.; Jao, M.-H.; Darling, S. B.; Su, W.-F. Additives for Morphology Control in High-Efficiency Organic Solar Cells. *Mater. Today* **2013**, *16*, 326−336.
(47) Fabiano, S.; Himmelberger, S.; Drees, M.; Chen, Z.; Altamimi, R. M.; Salleo, A.; Loi, M. A.; Facchetti, A. Charge transport Orthogonality in All-Polymer Blend Transistors, Diodes, and Solar Cells. *Adv. Energy Mater.* **2014**, DOI: 10.1002/aenm.201301409.
(48) Tremel, K.; Fischer, F. S. U.; Kayunkid, N.; Pietro, R. D.; Tkachov, R.; Kiriy, A.; Neher, D.; Ludwigs, S.; Brinkmann, M. Charge Transport Anisotropy in Highly Oriented Thin Films of the Acceptor Polymer P(NDI2OD-T2). *Adv. Energy Mater.* **2014**, *4*, n/a.
(49) Chen, W.; Nikiforov, M. P.; Darling, S. B. Morphology Characterization in Organic and Hybrid Solar Cells. *Energy Environ. Sci.* **2012**, *5*, 8045.

DOI: 10.1021/acsami.5b04224
ACS Appl. Mater. Interfaces 2015, 7, 15995−16002